

# Effects of Sampling Interval on the Frequency-Magnitude Relationship of Rockfalls Detected from Terrestrial Laser Scanning using Semi-Automated Methods

Megan van Veen<sup>1</sup>, D. Jean Hutchinson<sup>1</sup>, Ryan Kromer<sup>1</sup>, Matthew Lato<sup>2</sup>, Tom Edwards<sup>3</sup>

<sup>1</sup> Department of Geological Sciences and Geological Engineering, Queen's University, Kingston, ON, Canada, K7L 3N6

<sup>2</sup> BGC Engineering Inc., 414 Princeton Ave., Ottawa, ON, Canada L2A 4G2

<sup>3</sup> Canadian National Railway, 10229-127 Avenue, Edmonton, AB T5E 1B5

Corresponding Author: Megan van Veen ([m.van.veen@queensu.ca](mailto:m.van.veen@queensu.ca), (613) 532-5328)

## Abstract

Using change detection and semi-automated identification methods, it is possible to extract detailed rockfall information from terrestrial laser scanning data to build a database of events, which can be used in the development of the frequency-magnitude relationship for a slope. In this study, we have applied these methods to the White Canyon, a hazardous slope that presents rockfall hazards to the CN Rail line in British Columbia, to build a database of rockfalls including their locations, volumes, and block shapes. We identified over 1900 rockfall events during a 15-month period, ranging in volume from 0.01 to 45 m<sup>3</sup>. The frequency of these events changed throughout the year, with the highest periods of activity occurring over the winter months. We investigated how the sampling interval, or duration between scans, can affect how the rockfalls are identified, and therefore the frequency-magnitude relationship for the slope using datasets with fewer scans. We show that as the duration between scans becomes larger, fewer rockfalls are detected, as multiple events that have occurred in the same location cluster together into a single event. The results of this study can be used to assist the railways in planning the appropriate number and duration between future scans, in order to capture frequency-magnitude data for the slope with a desired level of detail.

## Keywords

Terrestrial Laser Scanning

LiDAR

Rockfall hazard

Rockfall frequency-magnitude

Change detection

## Acknowledgements

This research was supported by the Canadian Railway Ground Hazard Research Program (CN Rail, CP Rail, Transport Canada, Geological Survey of Canada). Support was also provided by BGC Engineering Inc. through the Natural Sciences and Engineering Research Council of Canada's Industrial Postgraduate Scholarship Program. Thanks are given to Matthew Ondercin

43 and Emily Rowe for their assistance in data collection as well as staff from the Kumsheen  
44 Rafting Resort for providing logistical support and site access.

## 45 Introduction

46 The frequency-magnitude relationship of rockfalls is an important component of hazard and risk assessment  
47 for dangerous slopes, which can be evaluated through the use of a rockfall database. In the case of rock slopes along  
48 rail lines, these inventories have been traditionally created through collection of data during track inspections. On  
49 slopes where activity is frequent, it can be difficult to maintain a complete record, especially for smaller events that  
50 may not be identified at track level. These inspections require railway personnel to be directly exposed to the hazard  
51 (Lato et al. 2009). On large, complex slopes, such as those along the railways in Western Canada, it can also be  
52 difficult to identify rockfall source zones in the field, due to obstructed line of sight and visually complex slopes.  
53 However, information on rockfall source zones, such as the location of the source zone and shape of the block can  
54 be useful in addition to the frequency-magnitude relationship for understanding the failure processes operating on  
55 the slope (Ritchie 1963). Remote sensing methods can be advantageous where steep and unstable slopes render  
56 typical field data collection unsafe and unfeasible (Sturzenegger and Stead 2009).

57 Terrestrial laser scanning (TLS) can be a useful tool in characterizing the changes over time on rock slopes.  
58 By performing change detection using multi-epoch, sequential scans, individual rockfall events can be identified on  
59 the slope, including their locations and volumes, as demonstrated by Rosser et al. (2007), Lato et al. (2009), Lim et  
60 al. (2010), and Abellán et al. (2010). Hungr et al. (1999) determined that there is a demonstrated relationship  
61 between rockfall volume and cumulative rockfall frequency which can be defined by a power law such that:

$$62 \quad f(V) = \alpha V^{-b}$$

63 where  $f(V)$  is the cumulative number of rockfalls,  $V$  is the rockfall volume, and  $\alpha$  and  $b$  are constants. This  
64 relationship appears as a straight line when plotted on a log-log graph. Many studies, including Rosser et al. (2005),  
65 Santana et al. (2012), D'Amato et al. (2013), and Guerin et al. (2014) have shown that the rockfall  
66 frequency-magnitude relationship for slopes can be determined through the use of TLS and that these relationships  
67 are generally well fit by a power law.

68 Santana et al. (2012) show that the frequency-magnitude relationship can be calculated with a  
69 semiautomated method using areas of rockfall scars and exposed discontinuity surfaces to estimate rockfall volumes.  
70 D'Amato et al. (2013) use a similar process for determining the shape of fallen blocks based on the orientations of  
71 joint planes. Both studies show a power law fit for the frequency-magnitude plot of the rockfalls for volume ranges  
72 greater than  $0.25 \text{ m}^3$  and  $0.1 \text{ m}^3$  respectively. Both studies identify an undersampling of smaller events, causing a  
73 “rollover” in the frequency-magnitude curves.

74 Guerin et al. (2014a) completed a study where rockfalls were identified using TLS on a large cliff in  
75 Grenoble, France, over a three-year period and their volumes were calculated by creating 3D meshes of the rockfall  
76 regions. For this particular study, the limit of detection for change was 10 cm and the rockfall data was well fit by a  
77 power law for volumes greater than  $0.05 \text{ m}^3$ . However, they noted that this process was quite manual and time  
78 consuming.

79 Tonini and Abellán (2014) present a method for automatically identifying changes and clustering points  
80 corresponding to each rockfall using point cloud data. Using this method, a distance threshold is set to extract  
81 rockfall features from the change detection data. A nearest neighbour clutter removal algorithm (Byers and Rafferty  
82 1998) is then applied to this data in order to separate rockfall features from any residual noise or clutter in the data.  
83 A density based spatial clustering application (DBSCAN, Ester et al. (1996)) is used to separate the remaining points  
84 into clusters representing each rockfall event. In this study, the number of points making up a rockfall cluster was  
85 used as an analogue for volume in analyzing the frequency-size distribution of rockfalls. Carrea et al. (2015) identify  
86 that previous methods of calculating rockfall volumes based on scars may not be sufficient when dealing with  
87 geometrically complex slopes where rockfall shapes are not regular (blocks are not clearly bounded by regular joint  
88 surfaces). In a study of La Cornalle cliff in Switzerland, the techniques outlined by Tonini and Abellán (2014) are  
89 applied to identify rockfall events and their volume is calculated using an alpha-shape concave hull method  
90 (Edelsbrunner and Mucke (1994), Teichmann and Capps (1998)) to calculate the volume of the complex, concave

91 shaped rockfalls. Using these methods, rockfalls were identified and the dataset had a frequency-magnitude  
92 relationship that was well fit by a power law for volumes greater than 0.1 m<sup>3</sup>.

93 Tonini and Abellán (2014) and Carrea et al. (2015) note that using too long of an interval between scans  
94 may lead to the overlapping of multiple events, causing them to be interpreted as one single event. This may affect  
95 the frequency magnitude- relationship, and the temporal variability in events must be considered in future work.  
96 Janeras et al. (2015) present the successful application of similar techniques to the study of rockfalls in the  
97 Montserrat Massif in Spain and also identify the need for increased sampling frequency to understand the time  
98 variability of the results.

## 99 Study Objectives

100 The objectives of this study are to apply the methods outlined above and build on these in order to identify  
101 rockfalls on a large, complex slope. We also use these methods to develop an understanding of how sampling  
102 interval (duration between scans) affects the results of the rockfall identification and the resulting  
103 frequency/magnitude relationship, considering the high frequency of events recorded on this slope. A longer  
104 sampling interval may cause individual rockfall events, occurring at different times in the same location to coalesce,  
105 thus appearing as a single event in terms of the automatic classification. We also demonstrate how a classification of  
106 rockfall block shape can be incorporated into this process and discuss how these results can be incorporated into  
107 further hazard analysis. This analysis may lead to a better understanding of how often, and when data should be  
108 collected in order to create a complete and accurate record of rockfall activity on the slope, which can be used as  
109 input to the Canadian National (CN) Railway's rockfall hazard management process.

## 110 Study Site

111 The White Canyon is located just outside the town of Lytton, British Columbia in Canada and spans a 2.2  
112 km section of railway between Milepost 93.1 to 94.6 of the CN Ashcroft subdivision (Figure 1). The rocks in the  
113 canyon are highly weathered and foliated, and the complexity of the rock mass produces rockfalls varying in size  
114 and shape. The predominant lithology in the canyon is a quartzofeldspathic gneiss which contains a series of tonalite  
115 dykes and dioritic intrusions (Brown 1981). Many of these intrusions form vertical spires on the slope which act as  
116 source zones for rockfalls. Notable failures in recent history at this site include a 2600 m<sup>3</sup> event which occurred in  
117 June 2013, which is discussed in detail, along with the geology and structure of the slope by Kromer et al. (2015b).  
118 Frequent rockfall activity presents a hazard to the railway as it is built in close proximity to the Thompson River and  
119 there is limited space for rockfalls to accumulate in the ditches at the bottom of the slope. Consequently, ditch  
120 maintenance must take place on a regular basis. In addition, a series of rock sheds are used to collect and/or direct  
121 debris over the track in certain areas. While activity on this slope is frequent, the rockfall records have not been  
122 well-maintained, which limits the analysis of relationships with this data.

123 The canyon is separated into two sections by a short railway tunnel and the results of this study are focused  
124 on the West half of the canyon. We have studied this slope using remote sensing methods (terrestrial and aerial  
125 LiDAR, Gigapixel photography, and photogrammetry) since 2012 and have refined data collection methods over  
126 this period to collect high resolution data over the entire slope (approximately 1 km wide by 600 m tall) such that we  
127 can consistently identify small volume rockfalls (0.01 m<sup>3</sup>) across the entire slope.

128 **Fig 1. a) Map outlining location of the White Canyon in southwestern British Columbia b) coloured**  
129 **photogrammetry model of the White Canyon West slope created using data collected in September 2013 c)**  
130 **image of the slope taken looking up when standing at track level (Mile 93.2).**

## 131 Methods

### 132 Data Collection

133 TLS data was collected on 7 dates between November 2014 and February 2016 (6 scan intervals, 15 months  
134 total) using an Optech ILRIS-3D scanner with enhanced range capabilities. Data was collected from five sites on the  
135 opposite bank of the Thompson River. The locations of these sites were optimized based on experience from scans  
136 in the previous years in order to minimize poor incident angles. At each site, data was collected using a series of

137 tiled boxes for the lower, middle, and upper portions of the slope, with overlap between boxes. This was done in  
138 order to achieve a more consistent point spacing over the entire height of the slope. The Optech scanning device  
139 requires the user to set an internal angle within the system to achieve a given point spacing at a given distance, and  
140 this angle does not change with distance. Therefore, the point spacing is smaller than specified at the bottom of each  
141 box, and larger than specified at the top. By breaking the scan into separate boxes (Figure 2), we can specify a  
142 different angle for each box. An average distance and target point spacing are set for each box (Table 1) such that the  
143 overall difference in point spacing across the slope is minimized (maximum difference of 0.041 m in the case of this  
144 scan site) compared to if a single scan box was used.

In addition to the TLS data, high-resolution images were collected using a Nikon D800 camera and a Gigapan Epic Pro robotic head (Lato et al. 2012). These images were stitched together such that known rockfall events could be located in the images. A set of photos taken in September 2013 were also available for creating a high resolution photogrammetric model of the slope, using PhotoScan (Agisoft 2015) and methods described by Tavani et al. (2014). This model could be used to manually classify the slope into areas of rock outcrop and areas of talus channels.

**Fig 2. Comparison of TLS survey design in the White Canyon using a single scan box vs. multiple boxes to create a more even distribution of point spacing across a large slope**

**Table 1. Scan distance and point spacing comparison for the case of multiple boxes shown with overlap**

	<b>Box 1</b>	<b>Box 2</b>	<b>Box 3</b>
<b>Specified Distance</b>	600 m	500 m	400 m
<b>Specified Point Spacing</b>	9.80 cm	10.0 cm	9.60 cm
<b>Scan Average Distance</b>	545 m	420 m	344 m
<b>Point Spacing at Average</b>	8.71 cm	8.40 cm	8.27 cm
<b>Point Spacing Range</b>	7.09 to 11.21 cm	7.39 to 10.50 cm	7.37 to 9.47 cm

## TLS Data Processing

Prior to the processing of data to extract rockfall information, data treatment took place, which included cleaning, alignment, and masking. The raw point clouds were manually cleaned using PolyWorks PifEdit (InnovMetric 2015) to remove heavily vegetated areas as well as individual trees on the slope.

Following this, scans were aligned to a common coordinate system, using the data from November 2014 as a reference. In addition to aligning each of the 7 scans to the previous data (Date Set 4 in Figure 3), we created three synthetic datasets with fewer scans (Date Sets 1-3 in Figure 3). Corresponding scans were aligned to a previous date, but not necessarily the closest date, to mimic a scenario where scans were collected with longer durations in between, in order to investigate the effects of sampling period on the results of the automatic rockfall classification. For example, in Date Set 2, the scans from June 2015 were aligned to November 2014, and scans from February 2016 were then aligned to June 2015. Because of the large size of the slope, the model was split into three sections. The alignment was performed using the IMAAlign module of PolyWorks, first by manually picking three pairs of common points between the models, and then using an Iterative Closest Point (ICP) best-fit algorithm (Besl & McKay, 1992; Chen & Medioni, 1991). To improve the alignment, areas of known change (primarily talus channels) and areas of poor incidence angle in the upper slope were selected and ignored during the alignment process.

**Fig 3. Outline of the four date sets used for change detection and automatic rockfall identification including number of scans used and duration between scans**

31

32

33

The slope at the White Canyon is made up of complex features that contain both rock outcrops and talus channels, and analysis of change on the slope in previous years has shown that the talus channels behave differently 34 than the areas of rock outcrop, as would be expected. In areas of rock outcrop, individual blocks detach and move

35

time. Therefore, 36

extracting rockfalls 37

classifying a model of the 38

the areas of outcrop. 39

same areas were 40

In contrast, the talus channels often build up material which moves downslope over time. Therefore, 36 we manually masked out all areas of talus on the slope, such that the automated procedure for extracting rockfalls 37 would not pick up any of the larger scale talus movement. This process was completed by classifying a model of the 38 slope, made with photogrammetry, into areas of outcrop and talus, then extracting only the areas of outcrop. 39 Following this, the model of outcrop areas was overlain on the aligned point clouds such that the same areas were 40 masked in each cloud (Figure 4).

41

**Fig 4. Masking of non-outcrop areas using classified photogrammetry model to prepare model for 42 automatic rockfall detection – a) TLS model, b) photogrammetric model, c) photogrammetric model 43 classified by talus and outcrop, and d) TLS model with areas of talus masked out.**

## 1 Analysis: Volume Extraction and Classification

2 The processing of the TLS point clouds to extract rockfall information includes the following steps (Figure 5)  
3 which are described in detail in later sections:

- 4 a) Change detection between the reference and comparison date.
- 5 b) Filtering of change detection results using change threshold and merging of two models.
- 6 c) Clustering of rockfalls using DBSCAN method (Ester et al. 1996).
- 7 d) Calculation of rockfall volumes and block shapes.
- 8 e) Final filtering to remove vegetation and unwanted edge effects.

9  
10 **Fig 5. Summary of methods used for automated rockfall detection and volume calculation.**

### 11 Change Detection and Noise Filtering

12 The change detection process used is outlined in detail in Kromer et al. (2015a). Distances between point  
13 clouds were calculated along a slope dependent normal vector (Lague et al. 2013) and a spatial noise filter was  
14 applied to the raw distances (Abellán et al. (2009), Kromer et al. (2015a)).

15 In order to define both the front and back of each rockfall shape, this change detection is completed twice  
16 for each set of comparison dates (for example using Date A as a reference and Date B as the comparison cloud, and  
17 then using Date B as the reference and Date A as the comparison cloud). A detectable change threshold of 5 cm was  
18 set based on the standard deviations of the alignments between each of the point clouds for all of the dates that were  
19 considered. We then filter out any change less than +/- 5 cm such that the remaining product is a set of points  
20 containing clusters of points representing rockfalls and a small amount of residual outliers.

### 21 Rockfall Identification and Volume Calculation

22 The remaining points are separated into individual rockfall clusters using the DBSCAN algorithm in  
23 MATLAB (MathWorks 2015). A search radius of 0.3 m and minimum number of 12 points were determined to be  
24 appropriate values for this slope and data density. Using a smaller search radius and fewer points caused the front  
25 and back portions of some rockfalls to be separated into two distinct clusters, while using a larger radius and number  
26 of points resulted in some small rockfalls being identified as noise.

27 Using each cluster of points, the centroid of each rockfall can be identified and the volume of each block is  
28 calculated using the 3D alpha-shape method (Edelsbrunner and Mucke 1994). For each block, a unique alpha shape  
29 radius was set in order to minimize the presence of holes during the creation of the shape, which sometimes occur  
30 due to the complex geometry of the shapes (Figure 6). The radius was selected for each rockfall based on a  
31 relationship determined using the size of each rockfall. Taking advantage of the detailed set of 3D points making up  
32 each rockfall, we are able to calculate the short, long, and intermediate dimensions of each block and can add this  
33 shape information to our database of rockfall events.

34 **Fig 6. Example of alpha shape used to calculate rockfall volume with a) holes in shape leading to**  
35 **underestimate of rockfall volume b) holes filled for more accurate volume estimate**

### 36 Rockfall Filtering

37 To further separate rockfalls from the many small shrubs that exist on the slope and any leftover clusters of  
38 noise, we applied a threshold on the minimum volume and minimum number of points required to confirm a rockfall  
39 event, which are 0.01 m<sup>3</sup> and 40 points. While it is possible to identify rockfalls smaller than this volume using the  
40 automated classification, it is not possible to distinguish these from many of the small bushes on the slope (which  
41 are difficult to completely remove from the data) without manually confirming the classification. To remove any  
42 residual noise (mainly edge effects from the change detection algorithm), we remove rockfalls where the cluster is  
43 primarily made up of points with only negative or only positive change, and therefore does not form a complete  
44 rockfall shape. To account for differences in surface roughness before and after the rockfall, and the presence of  
45 occlusions in the data, this allowable ratio of negative to positive or positive to negative points is set to three.

## 46 Results

47 **Rockfall Frequency-Magnitude Curves**

48 The process described above was first applied to the date set containing all of the available scans (Date Set  
49 4) to distinguish as many individual events as possible, and the time period during which they occurred. Using all of  
50 the individual scans from Date Set 4 (seven scans total) we identified 1982 rockfalls from the six different interscan  
51 periods, ranging in volume from 0.01 to 44.8 m<sup>3</sup>. The frequency-magnitude curve (Figure 7) shows a good power  
52 law fit for volumes greater than 0.03 m<sup>3</sup>. The baseline level of rockfall activity for the 18-month period was 2.7  
53 rockfalls per day (summer and fall months), with higher rates occurring in the spring (3.6 per day) and winters (5.6  
54 per day for winter 2014 and 5.9 per day for winter 2015).

55 **Fig 7. Frequency-magnitude results and rockfall rates for Date Set 4 (making use of all available data)**

57 **Comparison of Sampling Periods**

58 The same analysis was completed for Date Set 1, Date Set 2, and Date Set 3, in order to compare the results  
59 of the automatic rockfall detection and classification, to simulate the situation where fewer scans were collected. The  
60 frequency-magnitude plot for all four date sets is shown in Figure 8, and from this it appears that the data from Date  
61 Set 4 (7 scans) plots slightly higher than the rest of the data for smaller volumes (meaning a larger number of  
62 rockfalls detected) and the data from Date Set 1 (2 scans) plots slightly lower than the rest of the data in the same  
63 area. However, there does not appear to be a significant difference between each of the datasets when plotted in this  
64 manner. If we compare the power law fit for each of these datasets, it is evident that there is also not a significant  
65 difference in the equation of best fit between the four datasets (Table 2), with  $\alpha$  ranging from 43.07 to 44.98,  $b$   
66 ranging from 0.98 to 1.01, and the R<sup>2</sup> value ranging from 0.995 to 0.997. Both the  $\alpha$  and  $b$  values increased  
67 slightly with an increasing number of scans, while the range of this fit increased to include rockfalls greater than  
68 0.03 m<sup>3</sup> for Date Set 3 and 4, compared to rockfalls greater than 0.04 m<sup>3</sup> for Date Set 1 and 2.

69 Upon looking more closely, we can identify some difference in the four datasets, however this difference  
70 does not significantly influence the frequency-magnitude relationship because these differences occur primarily in  
71 the “rollover” portions of the graph (small magnitude range) that are not fit by the power law. If we plot this data on  
72 a histogram (Figure 9) it can be seen that there is a significant difference in the number of rockfalls for each dataset  
73 for the lower volume ranges, with the trend showing that if fewer scans are included, less rockfalls are detected in  
74 these lower ranges. This can be interpreted as a result of several rockfalls occurring in the same area coalescing into  
75 one apparent rockfall when the change detection occurs over a long period of time. This is demonstrated by the  
76 example shown in Figure 10. This difference may be significant for volumes less than 0.04, where the difference  
77 between Date Set 4 and Date Set 1 ranges from 527 rockfalls for the 0.01 m<sup>3</sup> bin to 246 rockfalls for the 0.03 m<sup>3</sup> bin.  
78 There appears to be no significant difference in the data from Date Set 1 and Date Set 2 for rockfalls greater than  
79 0.04 m<sup>3</sup> and very little difference between all datasets (+/- 1 rockfall) for volumes greater than 0.05 m<sup>3</sup>.

80 **Fig 8. Frequency-magnitude plot for all date sets**

81  
82  
83  
84  
85  
86  
87  
88  
89

**Table 2. Comparison of frequency-magnitude relationship power law equation and range of fit for the four date sets**

	<b>Date Set 1</b>	<b>Date Set 2</b>	<b>Date Set 3</b>	<b>Date Set 4</b>
<b># of Scans</b>	2	3	4	7

<b>A</b>	43.07	42.34	44.20	44.98
<b>b</b>	0.98	0.99	1.00	1.01
<b>R<sup>2</sup></b>	0.997	0.995	0.995	0.996
<b>Range of Fit</b>	0.04 m <sup>3</sup> and above	0.04 m <sup>3</sup> and above	0.03 m <sup>3</sup> and above	0.03 m <sup>3</sup> and above

90

91

92

**Fig 9. Histogram of rockfall frequencies comparing the four date sets. Inset shows the same data with different scale for number of rockfalls.**

93

94

95

96

**Fig 10. a) Change detection for a small section of track at Mile 94.6 between 2014-11-11 and 2016-02-15 (Date Set 1) showing many rockfall events clustered together b) Individual rockfall events identified using Date Set 4 in the same section, coloured by date.**

97

### Sampling Periods Based on Weather

98

99

100

101

102

103

104

105

106

107

108

109

110

111

112

113

114

When analyzing the listed causes of historical rockfalls along major railroads in Western Canada, 70% of events were noted to have occurred during periods of heavy precipitation and frequent freeze-thaw cycles (Wylie and Norrish 1996). Specifically in the Fraser Canyon, records have shown that rockfalls most frequently occur between October and March (Peckover 1975). We used an additional synthetic date set (similar to Date Sets 1-3) based on logical changes in the weather patterns of the area, which is herein denoted as Date Set W, to understand how the results would be affected if the scans were collected between seasonal changes, which may provide insight as to how the scheduling of scans could be better optimized. These dates are shown alongside temperatures and precipitation recorded at the Lytton weather station (Government of Canada 2016) during the study period (Figure 11). For this date set, we included scans taken in October and November (before freezing), as well as March, as these dates marked periods of time that had frequent freeze thaw cycles (winter) and periods where the temperature was consistently above zero (no freeze thaw cycles). We included a mid-winter scan from February 2015 in order to minimize the effects of any overlapping events at the same location over the winter, since it is known that the rockfall frequency is high during this period. The results of the rockfall detection for this additional dataset (5 scans) are shown alongside the results from Date Set 3 (4 scans) and Date Set 4 (7 scans) in Figure 12. From this, it can be seen that the results are very similar to Date Set 3 and that the results are the same as both Date Set 3 and Date Set 4 for rockfalls greater than 0.05 m<sup>3</sup>. However, there is still a difference in the results compared to if the maximum number of scans were included.

115

116

117

**Fig 11. Lytton temperature and precipitation data between 2014-11-11 and 2016-02-16 indicating scan dates used for Date Set W**

118

**Fig 12. Histogram of rockfall frequencies comparing Date Set W to Date Set 3 and 4**

119

### Rockfall Block Shapes

120

121

122

123

124

125

126

127

128

Using the dimensions of the blocks that were extracted during the automated rockfall detection, we organized the rockfalls into the classes outlined by Sneed and Folk (1958) which contain three endmembers: compact (cubic), platy (tabular), and elongated (rod shaped). These shapes are defined by the ratio of short to long and short to intermediate axis lengths of the particle, where a, b, and c represent the long, intermediate, and short axis lengths. These dimensions may be subject to some bias as we are only measuring the shape from a specific line of sight. Plots of the shape distributions for various volume ranges are shown in Figure 13. A histogram of the percentage of each shape per volume range is also included. From this it can be seen that for smaller magnitude rockfalls, there is a much higher percentage of rockfalls that fall into the cubic category, and this percentage decreases as volume increases. For the larger volume rockfalls, there is a larger range in the shapes of blocks

1 compared to smaller ones. Generally, there are very few rockfalls that fall into the VP (very platy), VB (very  
 2 bladed) and VE (very elongated) categories near the bottom of the chart, which is likely a result of a high degree  
 3 of  
 4 fracturing in the rockmass, preventing these shapes from occurring. It may also be possible that some of the larger  
 5 rod and tabular shaped rockfalls may be the result of several small rockfalls appearing as one due to the elapsed time  
 6 between successive scans. Upon closer inspection of the rockfalls that were classified as very platy (tabular) in the  
 7 change detection data and in photos, it appears that many of these events may have been a mass of talus-like  
 8 material sliding down the slope as opposed to being the result of the detachment of a solid block of rock that fell.

8 **Fig 13. a-d) Plot of rockfall block shapes for various ranges of rockfall volumes e) histogram**  
 9 **showing**  
 10 **percentage of rockfalls within each shape class for each volume range**

## 11 Discussion

12 The frequency-magnitude relationship for this rockfall dataset produced a b exponent of 1.01 with a good  
 13 power law fit for volume ranges from 0.03 m<sup>3</sup> up to 45 m<sup>3</sup> (maximum volume detected). In general, this  
 14 range of fit captures rockfall volumes smaller than the previously described studies (Table 3), with  
 15 a better fit, suggesting that  
 16 our careful survey planning and detailed processing techniques allow us to consistently and accurately identify  
 17 small rockfalls on the slope. The exception to this is the study presented by Dewez et al. (2013) where data was  
 18 collected  
 19 at a point spacing of 0.05 m (compared to approximately 0.1 m at White Canyon) over a smaller slope and the  
 20 power law fit was valid for volumes as small as 0.001 m<sup>3</sup>. It is also possible that, due to the geological setting of  
 21 the slope, the power law is valid for volumes smaller than other slopes. The b value of this dataset is slightly higher  
 22 than the previous studies. This observation may be attributed to the relatively small range of volumes identified  
 23 over the 15month period (no failures over 50 m<sup>3</sup>), the ability to detect much smaller rockfalls than some of these  
 24 other  
 25 studies, or the geological setting of the slope. Additional work on this slope has shown that the behavior of  
 26 rockfalls is variable depending on the source zone lithology, however the overall frequency-magnitude relationship  
 27 is dominated by the frequency of events in the quartzofeldspathic gneiss, which is the most dominant unit on the  
 28 slope (van Veen et al. 2016).

27 **Table 3. Comparison of frequency-magnitude relationship**  
 28 **for rockfalls detected using TLS compared**  
**to this study**

Study	Methods	b value	Range of Fit	R <sub>2</sub>
Santana et al. (2012) (Artificial Data)	Automated based on rockfall scars	0.92	0.25 to 1000 m <sup>3</sup>	0.987
Dewez et al., (2013) (2.5 years)	Based on 2.5D grid methods and erosion scars	0.54	0.001 to 100 m <sup>3</sup>	0.996
Guerin et al. (2014b) (3 years)	Manual detection	0.75	0.05 to 100 m <sup>3</sup>	0.994

Carrea et al. (2015) (2 years)	Automated detection	0.68	0.1 to 4 m <sup>3</sup>	0.973
White Canyon (15 months)	Automated detection	1.01	0.03 to 45 m <sup>3</sup>	0.996

29

30 Based on the comparison between the real datasets and the synthetic datasets created with fewer scan dates, 31  
it is evident that the highest level of detail can only be obtained using the maximum number of available scans, and

32 that there is some degree of overlap between events as the duration between scans becomes larger. As a result,  
there

33 are more of the smaller rockfalls and less of the larger events, producing a higher b value. As rockfalls begin to 34  
overlap, the calculation of their volume and centroid will also become less accurate. The railways can use this

35 information to determine what level of detail, and therefore frequency of scanning, is appropriate for  
their analysis.

36 While it may be possible to identify all individual events greater than a given magnitude with only one or two scans

1 a year, a record of all events, or better knowledge of the frequency of events is only available with a larger number  
2 of scans. D'Amato et al. (2016) studied a slope in Grenoble, France using TLS for a two-year period, and showed,  
3 by using high-resolution photographs with temporal frequency between 2 and 11 weeks, that less than 1% of  
4 rockfalls that were identified were a result of multiple events occurring in close proximity to each other, therefore a  
5 two-year scan interval may have been sufficient to identify all events on the slope. However, as demonstrated in this  
6 study, there are many cases of events overlapping in a shorter period (15 months) therefore multiple scans per year  
7 are needed to characterize each individual event. Previous studies have also shown that large failures on this slope  
8 are often preceded by a series of smaller failures around the perimeter of a larger block. An example of such  
9 phenomena is outlined in Figure 14, where a 2600 m<sup>3</sup> failure in the White Canyon is shown to have been preceded  
10 by 15 smaller events prior to failure. The frequency-magnitude diagram for these precursory failures shows a similar  
11 power law distribution on a smaller scale. A high density of scans in the time leading up to failure allowed each of  
12 these smaller events to be identified.

13 **Fig 14. a) outline of 2600m<sup>3</sup> failure that occurred on June 5<sup>th</sup> 2013 in the White Canyon with**  
14 **precursory events and their timing identified b) frequency-magnitude plot for 2600m<sup>3</sup> failure and 15**  
15 **precursory events**

16 However, if constrained to fewer data collection campaigns, separating the winter and summer seasons may  
17 be a logical decision, as the rates of rockfall activity decrease during the summer months. The frequency of events is  
18 high during the winter, and it is possible that there may be overlap of events during the winter months that we have  
19 been unable to capture in this study. An additional dataset from the winter months may help to better understand the  
20 high number of events occurring during this period, however the operation of the scanner in cold weather and  
21 decreased quality of data on wet and snow-covered slopes may not permit this. While it may be possible to obtain a  
22 complete record of all the events occurring on the slope with a few scans per year, more frequent, scans may help to  
23 better characterize the true frequency of events, which may be useful in predictive studies, or in correlating rockfall  
24 activity to triggering factors such as precipitation, freeze-thaw cycles, and seismic events. D'Amato et al., (2016)  
25 have shown that using shorter sampling intervals allows for a better correlation of rockfalls to triggering factors,  
26 including different components of freeze-thaw cycles and precipitation of varying duration and intensity.

27 In calculating the rockfall volumes, we selected a unique alpha-radius based on the maximum amount of  
28 change that occurred within each block. This is done in order to minimize the number of holes within the shape due  
29 to insufficient data density, or occlusions in the data, which are especially common in rockfalls originating from the  
30 large vertical spires in White Canyon. Any remaining holes in the rockfall shape may lead to an underestimate of  
31 rockfall volume, while using too large of a radius may cause an overestimate of volume. For a sample set of  
32 manually selected rockfalls, the average difference in volume using a manually selected, optimal alpha-radius for  
33 each rockfall, compared to the automatically selected one was 0.02 m<sup>3</sup> for rockfalls less than 0.5 m<sup>3</sup>, 0.17 m<sup>3</sup> for  
34 rockfalls between 0.5 and 1 m<sup>3</sup>, and 2.13 m<sup>3</sup> for rockfalls between 1 m<sup>3</sup> and 26 m<sup>3</sup>. While these differences may  
35 appear to be significant, Olsen et al. (2015) performed a study to investigate the effects of hole-filling in the 3D data  
36 prior to the detection of rockfalls and subsequent volume calculation and found that hole filling may not have a  
37 significant effect on the overall frequency-magnitude relationship. While they found the hole filling process useful  
38 in capturing larger rockfall events that were split into two by occlusions, we have not identified this as a problem in  
39 our datasets. The accuracy of the computed volumes may also be affected by the shape of the block, as we are using  
40 a threshold of 5 cm for the change detection, therefore removing a small amount of data from the outer edges of each  
41 block. Therefore, blocks with a larger surface area (platy and elongated blocks) may have a larger volume area than  
42 those that are cubic. From a hazard or risk assessment perspective these volume errors may not be significant, as the  
43 ability to calculate the approximate volume of rockfalls based on the actual source zone and model shape in itself  
44 provides a much higher level of detail compared to the process of estimating the volume from rockfall scars or  
45 debris from track level.

46 In addition to the frequency-magnitude relationship for the slope, this method of rockfall detection can  
47 provide additional information that may be useful in hazard analysis for the railway, including an understanding of  
48 where and when events are occurring across the large slope, in order to plan for maintenance activity, such as ditch  
49 clearing, or to design new mitigation or hazard management systems. The incorporation of rockfall block shape in  
50 the calculation is a simple addition to this process that can be used as input for rockfall modeling. The runout  
51 distance, rockfall velocity, and point at which the rockfall movement transitions from bouncing to rolling are all

52 influenced by rockfall block shape (Petje and Mikos 2005). As demonstrated by Kim Huyn et al. (2015), rock shape  
53 can influence the direction of rockfall trajectories using 3D modeling software. While it is not usually possible to  
54 determine the ending location of a rockfall event detected from the remote sensing data, given the known location of  
55 the rockfall source zone, the rockfall volume, as well as a basic idea of the rockfall block shape, it may be possible  
56 to model a set of known events, in order to determine the likelihood that these events make it to track level, and  
57 where they may end up, which can be of use to the railway, as the amount of rockfalls reaching track level is  
58 important for hazard assessment.

## 59 Conclusions

60 The use of TLS, careful survey design and processing, and a semi-automated analysis allows us to identify  
61 rockfall events on large slopes, where track-level data collection may not permit such detailed information to be  
62 collected. Using seven TLS datasets we are able to identify rockfalls for which the frequency-magnitude relationship  
63 can be fit by a power law for volumes greater than 0.03 m<sup>3</sup>. In considering longer duration scanning periods, we  
64 demonstrate that increasing the duration between scans can affect the rockfall detection, as rockfalls begin to overlap  
65 spatially over time, and that these effects are the most significant for the smaller volume rockfalls. However, the  
66 influence on the parameters of the frequency-magnitude relationship is very low. We also demonstrate that the  
67 distribution in rockfall block shapes changes depending on rockfall volume, and this can be a useful addition to  
68 rockfall modeling. Ultimately, using these methods, we are able to provide an improved database of the rockfall  
69 hazards on this slope when compared to the records that currently exist as well as an understanding of how the  
70 duration between scans affects the level of detail in rockfall volumes that can be contained in this database.

71

## 72 References

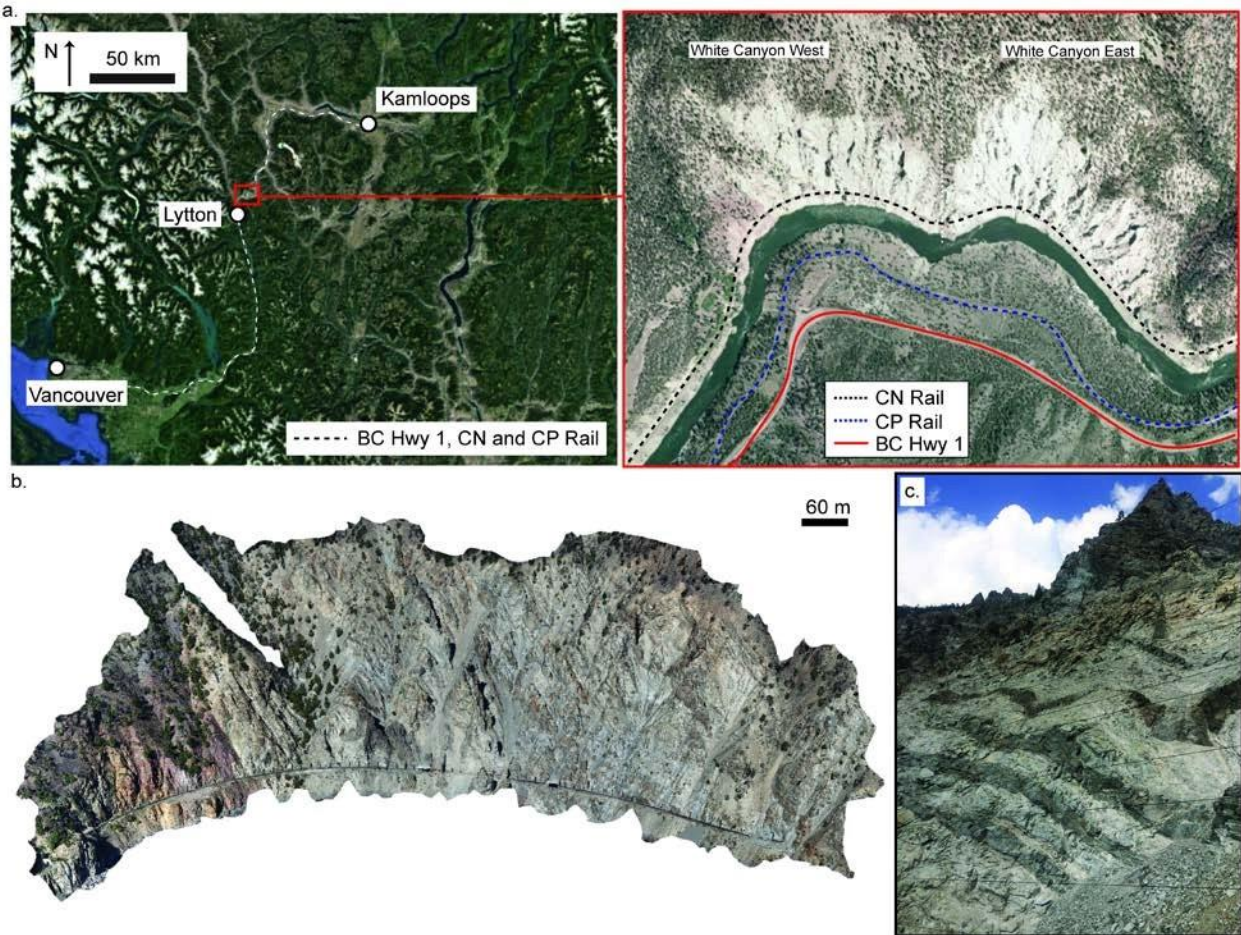
- 73 Abellán A, Calvet J, Vilaplana J, Blanchard J (2010) Detection and spatial prediction of rockfalls by means of  
74 terrestrial laser scanner monitoring *Geomorphology* 119:162-171 doi:10.1016/j.geomorph.2010.03.016
- 75 Abellán A, Jaboyedoff M, Oppikofer T, Vilaplana J (2009) Detection of millimetric deformation using a terrestrial  
76 laser scanner: experiment and application of a rockfall event *Natural Hazards and Earth System Science*  
77 9:365-372 doi:10.5194/nhess-9-365-2009
- 78 Agisoft (2015) Agisoft Photoscan Professional Edition v. 1.2.3.
- 79 Besl PJ, McKay ND (1992) A Method for the Registration of 3-D Shapes *IEEE Transactions on Pattern Analysis*  
80 and *Machine Intelligence* 14:239-256
- 81 Brown DA (1981) *Geology of the Lytton Area, British Columbia*. Carleton University
- 82 Byers S, Rafferty A (1998) Nearest-Neighbor Clutter Removal for Estimating Features in Spatial Point Processes  
83 *Journal of the American Statistical Association* 93:577-584
- 84 Carrea D, Abellán A, Derron M-H, Jaboyedoff M (2015) Automatic Rockfall Volume Estimation Based on  
85 Terrestrial Laser Scanning Data *Engineering Geology for Society and Territory* 2:425-428  
86 doi:10.1007/978-3-319-09057-3\_68
- 87 Chen Y, Medioni G Object Modeling by Registration of Multiple Range Images. In: *IEEE Conference on Robotics*  
88 and *Automation*, 1991.
- 89 D'Amato J, Guerin A, Hantz D, Rossetti JP, Jaboyedoff M (2013) Terrestrial Laser Scanner study of rockfall  
90 frequency and failure configurations. Paper presented at the Troisièmes Journées Aléas Gravitaires,  
91 Grenoble, France
- 92 D'Amato J, Hantz D, Guerin A, Jaboyedoff M, Baillet L, Miriscal A (2016) Influence of meteorological factors on  
93 rockfall occurrence in a middle mountain limestone cliff *Natural Hazards and Earth System Sciences*  
94 16:719-735
- 95 Dewez TJB, Rohmer J, Regard V, Cnudde C (2013) Probabilistic coastal cliff collapse hazard from repeated  
96 terrestrial laser surveys: case study from Mesnil Val (Normandy, northern France) *Journal of Coastal*  
97 *Research* 65:702-707
- 98 Edelsbrunner H, Mücke E (1994) Three-Dimensional AlphaShapes *ACM Transactions on Graphics* 13:43-72

- 99 Ester M, Kriegel H, Sander J, Xu X A Density-Based Algorithm for discovering clusters in Large Spatial Databases  
100 with Noise. In: 2nd International Conference on Knowledge Discovery and Data Mining, Portland, Oregon,  
101 1996.
- 102 Government of Canada (2016) Historical Climate Data - Environment Canada. climate.weather.gc.ca.
- 103 Guerin A, Hantz D, Rossetti JP, Jaboyedoff M (2014a) Brief communication "Estimating rockfall frequency in a  
104 mountain limestone cliff using terrestrial laser scanner" *Natural Hazards and Earth System Sciences*  
105 *Discussions* 2:123-135 doi:10.5194/nhessd-2-123-2014
- 106 Guerin A, D'Amato J, Hantz D, Rossetti J-P, Jaboyedoff M, (2014b) Investigating rock fall frequency using  
107 Terrestrial Laser Scanner Vertical Geology Conference, Lausanne, Switzerland p. 251-254
- 108 Hungr O, Evans SG, Hazzard J (1999) Magnitude and frequency of rock falls and rock slides along the main  
109 transportation corridors of southwestern British Columbia. *Canadian Geotechnical Journal*  
110 36:224338InnovMetric (2015) PolyWorks 2015 IR7.
- 111 Janeras M, Jara J, Lopez F, Marturia J, Royan M, Vilaplana J (2015) Using several monitoring techniques to  
112 measure the rock mass deformation at the Montserrat Masif. Paper presented at the International  
113 Symposium on Geohazards and Geomechanics,
- 114 Kim Huyn D, Gratchev I, Berends J, Balasubramaniam A (2015) Calibration of restitution coefficients using rockfall  
115 simulations based on 3D photogrammetry model: a case study *Natural Hazards* 78:1931-1946  
116 doi:10.1007/s11069-015-1811-x
- 117 Kromer R, Abellán A, Hutchinson D, Lato M, Edwards T, Jaboyedoff M (2015a) A 4D Filtering and Calibration  
118 Technique for Small-Scale Point Cloud Change Detection with a Terrestrial Laser Scanner *Remote Sensing*  
119 7:13029-13052 doi:10.3390/rs71013029
- 120 Kromer R, Hutchinson DJ, Lato M, Gauthier D, Edwards T (2015b) Identifying rock slope failure precursors using  
121 LiDAR for transportation corridor hazard management *Engineering Geology* 195:93-103  
122 doi:10.1016/j.enggeo.2015.05.012
- 123 Lague D, Brodu N, Leroux J (2013) Accurate 3D comparison of complex topography with terrestrial laser scanner;  
124 applications to the Rangitikei canyon (N-Z) *ISPRS Journal of Photogrammetry and Remote Sensing*  
125 82:1026
- 126 Lato M, Hutchinson DJ, Diederichs MS, Harrap R (2009) Optimization of LiDAR Scanning and Processing for  
127 Automated Structural Evaluation of Discontinuities for Rock Masses *International Journal of Rock*  
128 *Mechanics and Mining Sciences* 46:194-199
- 129 Lato MJ, Bevan G, Fergusson M (2012) Gigapixel Imaging and Photogrammetry: Development of a New Long  
130 Range Remote Imaging Technique *Remote Sensing* 4:3006-3021 doi:10.3390/rs4103006
- 131 Lim M, Rosser NJ, Allison RJ, Petley DN (2010) Erosional processes in the hard rock coastal cliffs at Staithes North  
132 Yorkshire *Geomorphology* 114:12-21 doi:10.1016/j.geomorph.2009.02.011
- 133 MathWorks (2015) MATLAB R2015b, 8.6.0.267246 edn.,
- 134 Olsen MJ, Wartman J, McAlister M, Mahmoudabadi H, O'Bannion M, Dunham L, Cunningham K (2015) To Fill or  
135 Not to Fill: Sensitivity Analysis of the Influence of Resolution and Hole Filling on Point Cloud Surface  
136 Modeling and Individual Rockfall Event Detection *Remote Sensing* 7:12103-12134  
137 doi:10.3390/rs70912103
- 138 Peckover FL (1975) Treatment of Rock Falls on Railay Lines *American Railway Engineering Association Bulletin*  
139 653:471-503
- 140 Petje UR, M., Mikos M (2005) Computer Simulation of Stone Falls and Rockfalls *Acta Geographica Slovenia*  
141 45:93-120
- 142 Ritchie AM (1963) Evaluation of Rockfall and its Control vol 17. Highway Research Board, Highway Research  
143 Record, National Academy of Sciences-National Research Council, Washington, DC
- 144 Rosser N, Lim M, Petley D, Dunning S, Allison R (2007) Patterns of precursory rockfall prior to slope failure  
145 *Journal of Geophysical Research* 112 doi:10.1029/2006jf000642
- 146 Rosser NJ, Petley DN, Lim M, Dunning SA, Allison RJ (2005) Terrestrial laser scanning for monitoring the process  
147 of hard rock coastal cliff erosion *Quarterly Journal of Engineering Geology and Hydrogeology* 38:363-375  
148 doi:10.1144/1470-9236/05-008
- 149 Santana D, Corominas J, Mavrouli O, Garcia-Sellés D (2012) Magnitude–frequency relation for rockfall scars using  
150 a Terrestrial Laser Scanner *Engineering Geology* 145-146:50-64 doi:10.1016/j.enggeo.2012.07.001

- 151 Sneed ED, Folk RL (1958) Pebbles in the Lower Colorado River, Texas a Study in Particle Morphogenesis The  
152 Journal of Geology 66:114-150
- 153 Sturzenegger M, Stead D (2009) Close-range terrestrial digital photogrammetry and terrestrial laser scanning for  
154 discontinuity characterization on rock cuts Engineering Geology 106:163-182  
155 doi:10.1016/j.enggeo.2009.03.004

1 Tavani S, Garanado P, Corradetti A, Girundo M, Iannace A, Arubes P (2014) Building a virtual outcrop, extracting  
 2 geological information from it, and sharing the results in google Earth via OpenPlot and Photoscan: An  
 3 example form the Khaviz Anticline (Iran) Computers & Geosciences 63:44-53  
 4 Teichmann M, Capps M Surface reconstruction with anisotropic density-scaled alpha shapes. In:  
 Proceedings of the 5 conference on Visualization '98, Los Alamitos, California, 1998. IEEE  
 Computer Society Press,  
 6 Tonini M, Abellán A (2014) Rockfall detection from LiDAR point clouds: a clustering approach using R Journal  
 of 7 Spatial Information Science 8:95-110  
 8 van Veen M, Hutchinson DJ, Gauthier D, Lato M, Edwards T (2016) Classification of Rockfall Patterns  
 using  
 9 Remote Sensing Data for Hazard Management in Canadian Rail Corridors Canadian Geotechnical 10  
 Conference, Vancouver Canada  
 11 Wylie DC, Norrish NI (1996) Stabilization of Rock Slopes. Transportation Research Board, National  
 Research  
 12 Council, Washington, D.C.  
 13 14  
 15

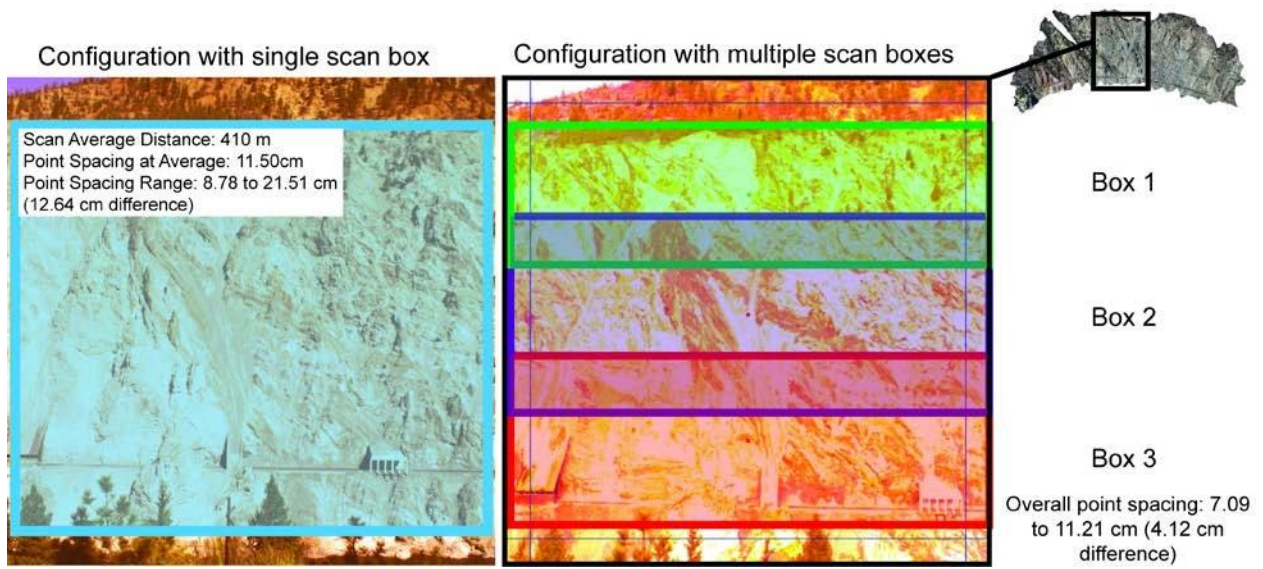
16 Fig.1



17  
 18

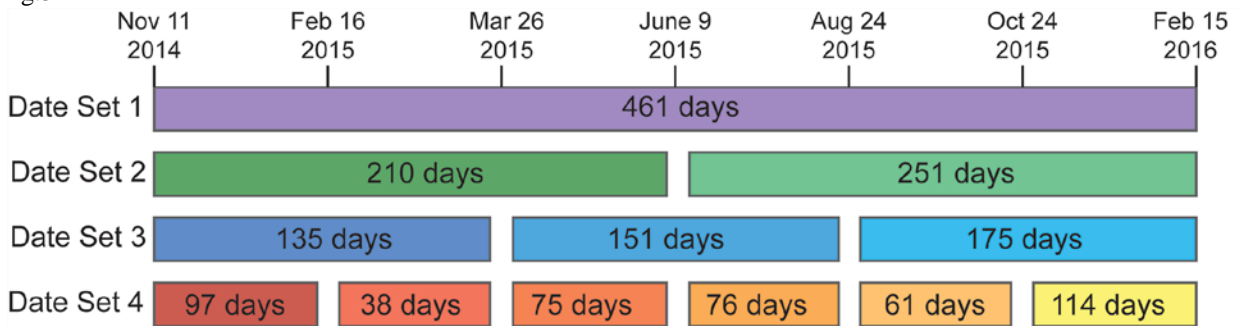
19  
20  
21

1 Fig.2



2  
3

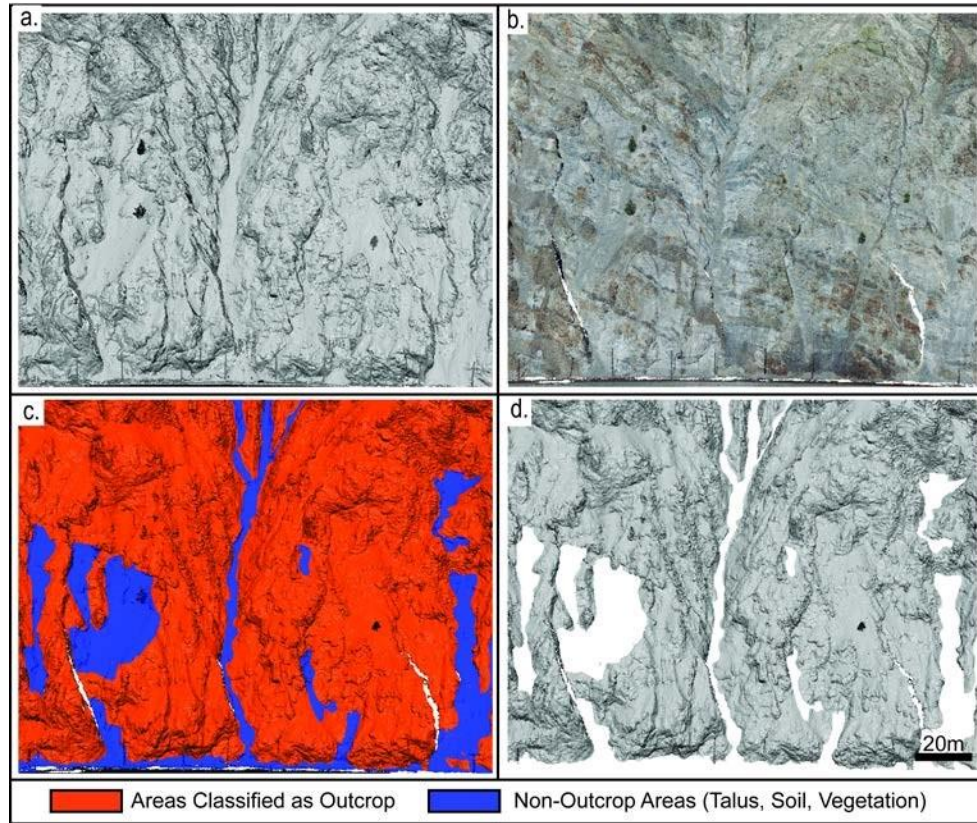
4 Fig.3



5  
6  
7  
8  
9  
10  
11  
12  
13  
14  
15  
16  
17  
18  
19

1

Fig.4



2

3

4

5

6

7

8

9

10

11

12

13

14

15

16

17

18

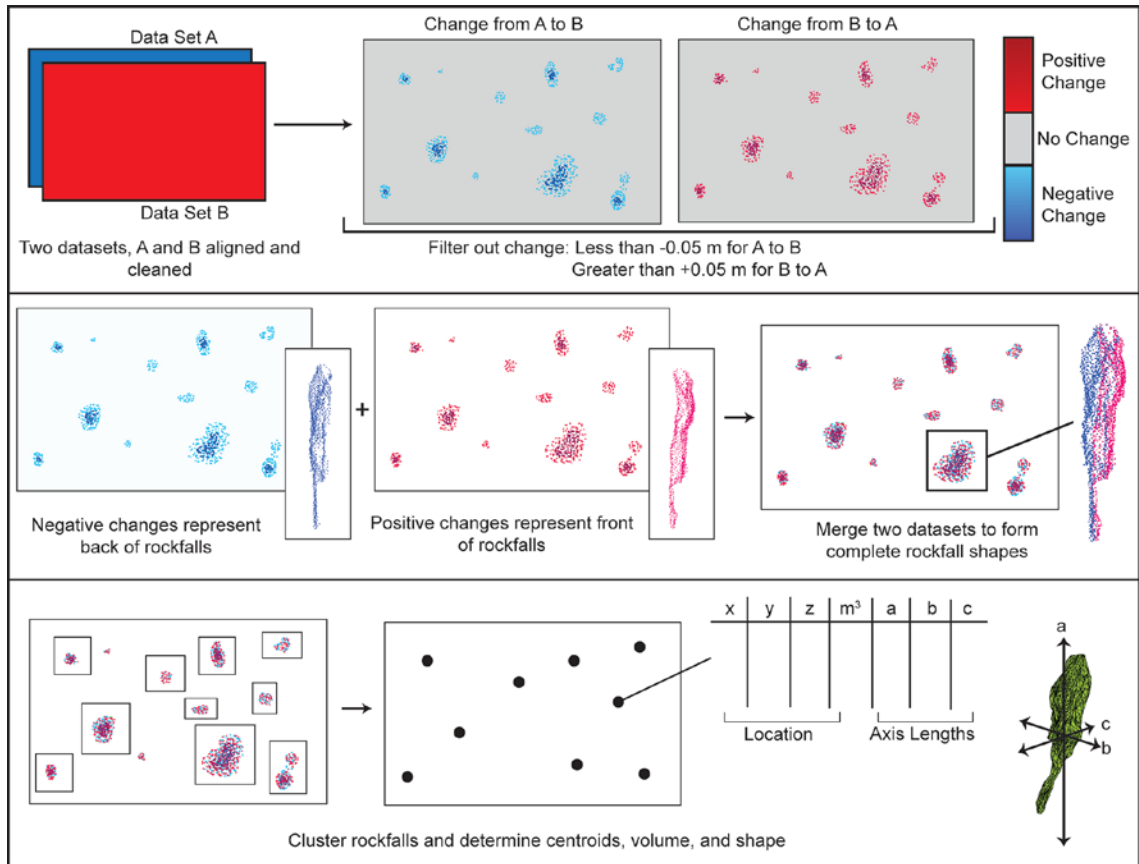
19

20

1

Fig.5

19

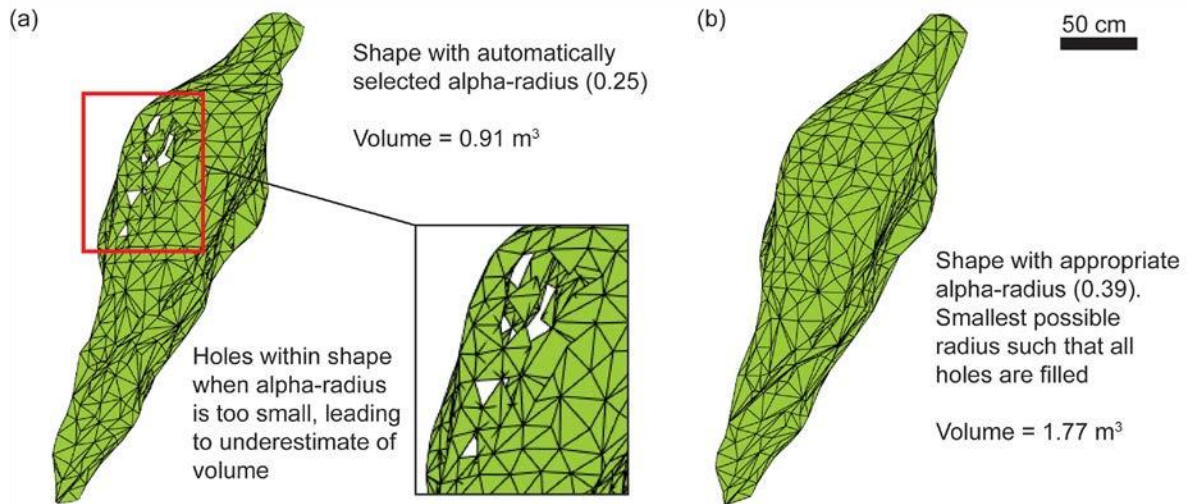


2

3

4

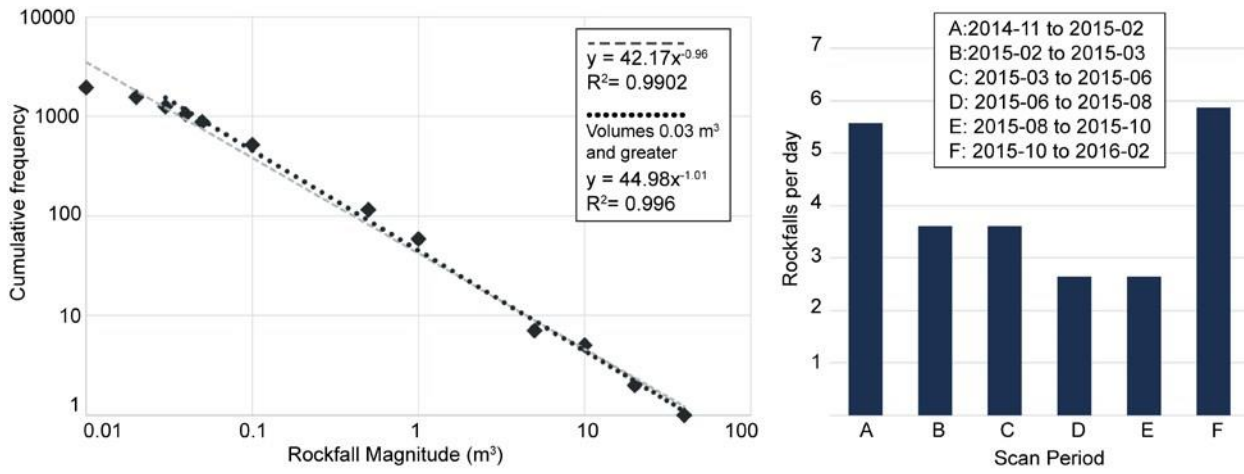
Fig.6



5

20

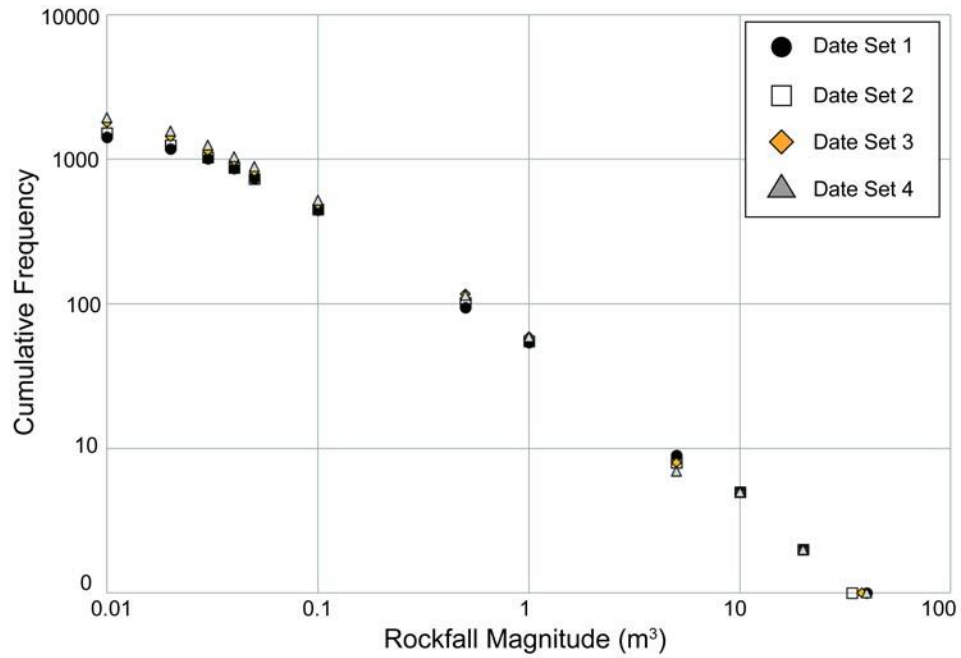
Fig. 7



2  
3

4

Fig. 8



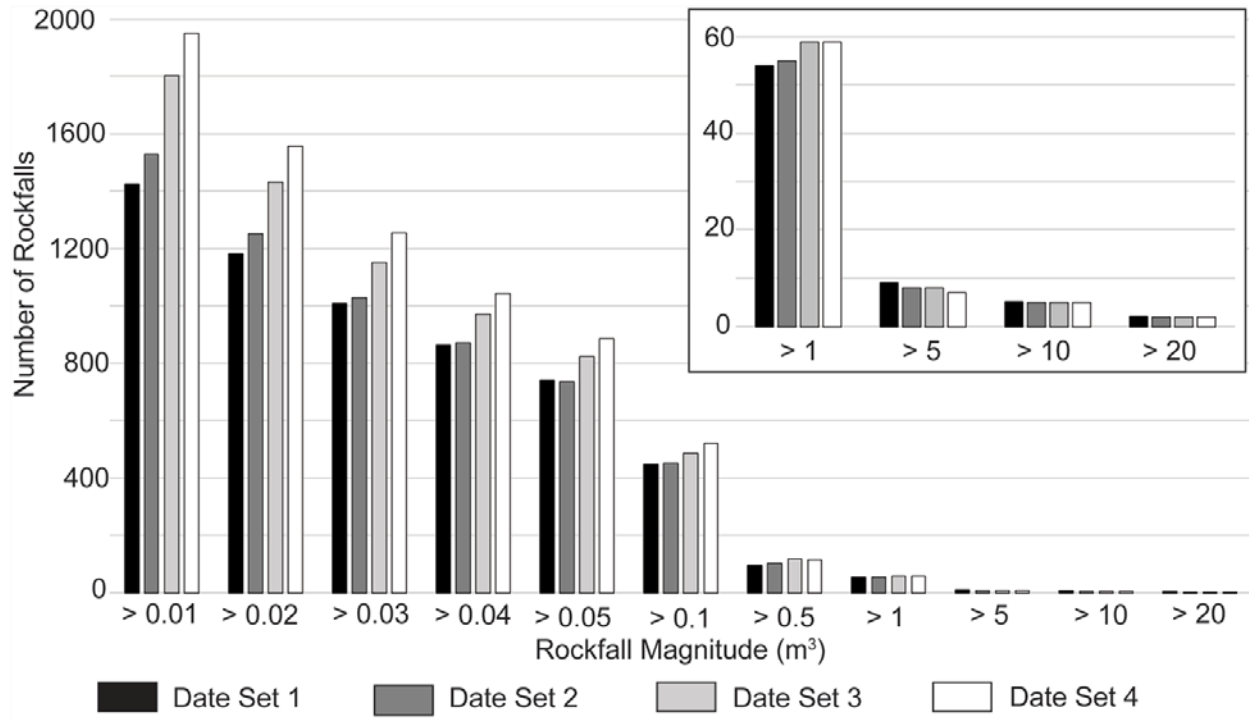
5

6  
7  
8  
9  
10  
11  
12  
13  
14

21

1

1 Fig. 9



2

3

4

5

6

7

8

9

10

11

12

13

14

15

16

17

18

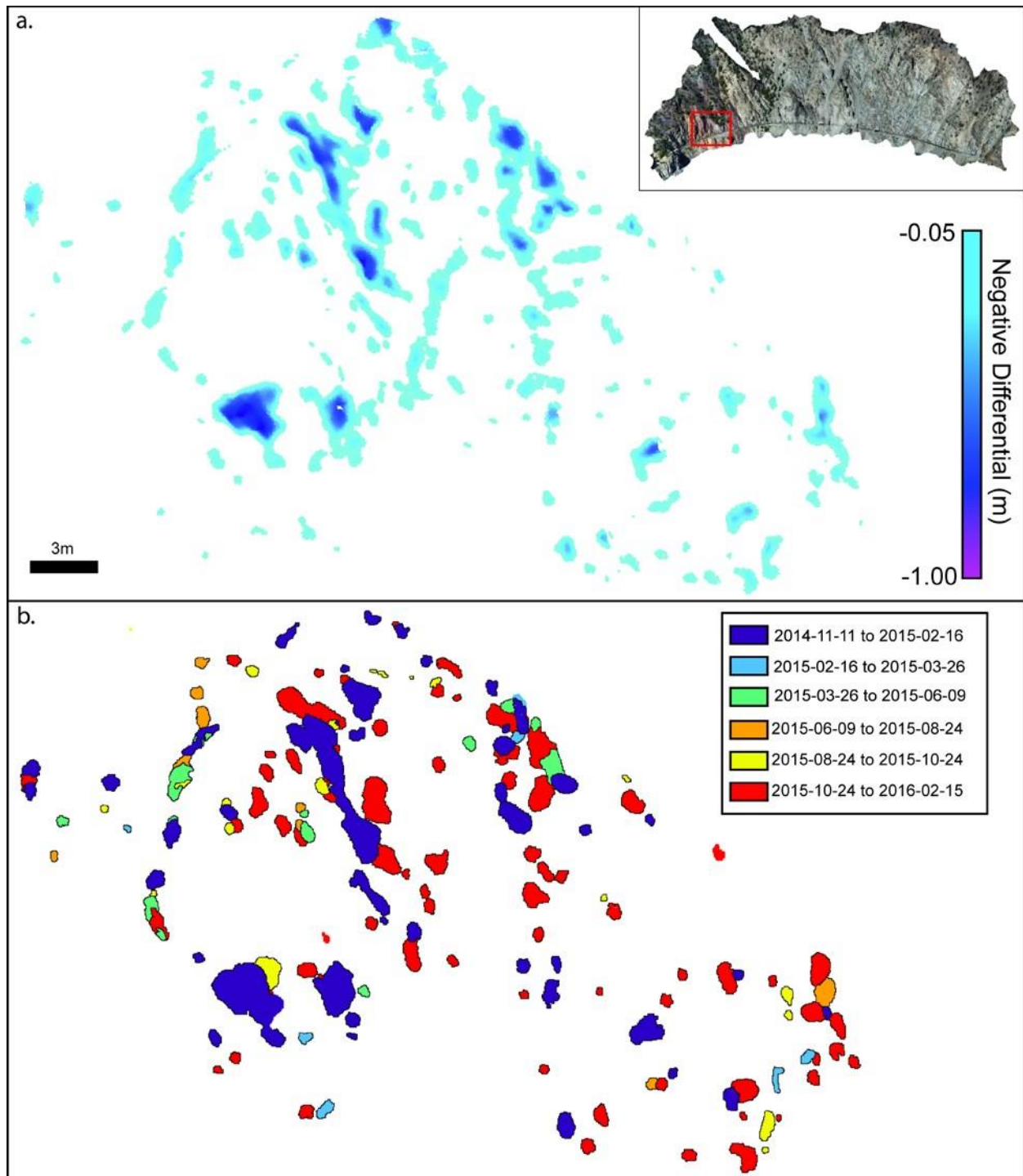
19

20

21

22

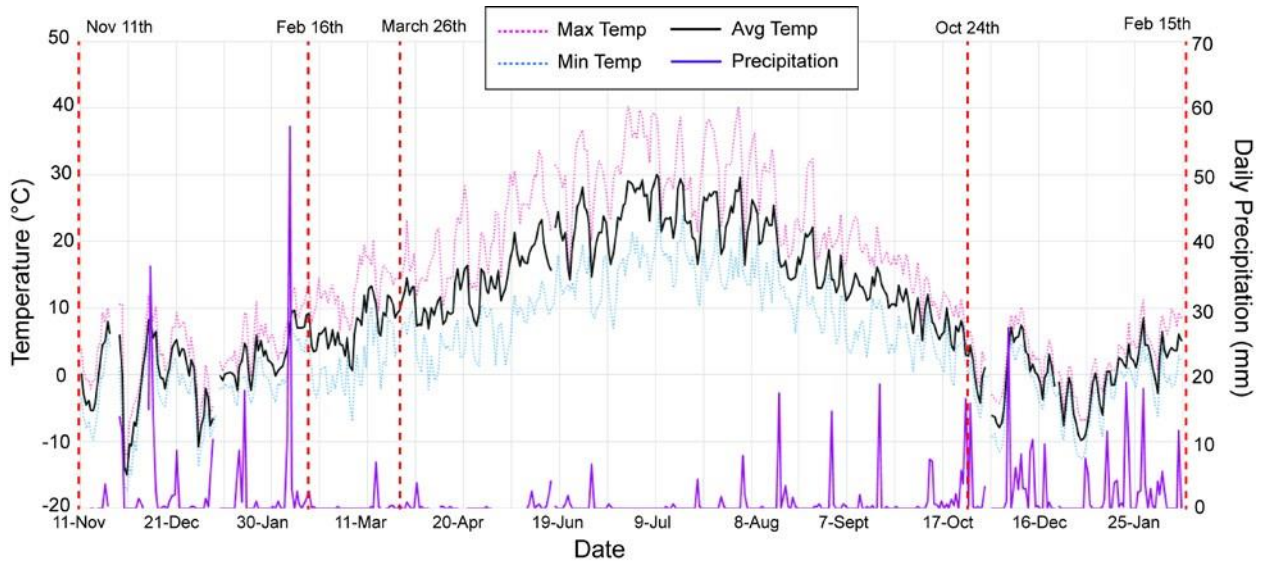
Fig. 10



2  
3  
4  
5  
6

1

Fig. 11

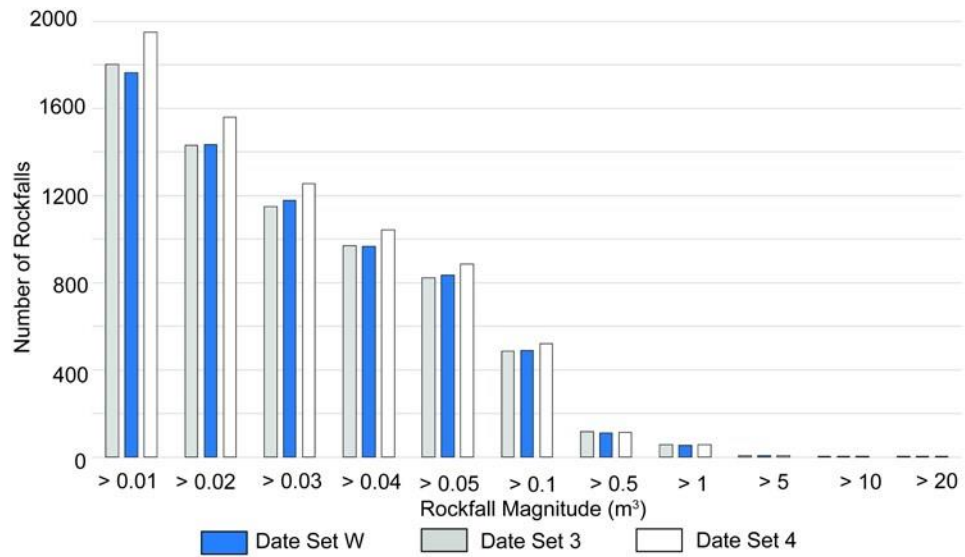


2

3

4

Fig 12.



5

6

7

8

9

10

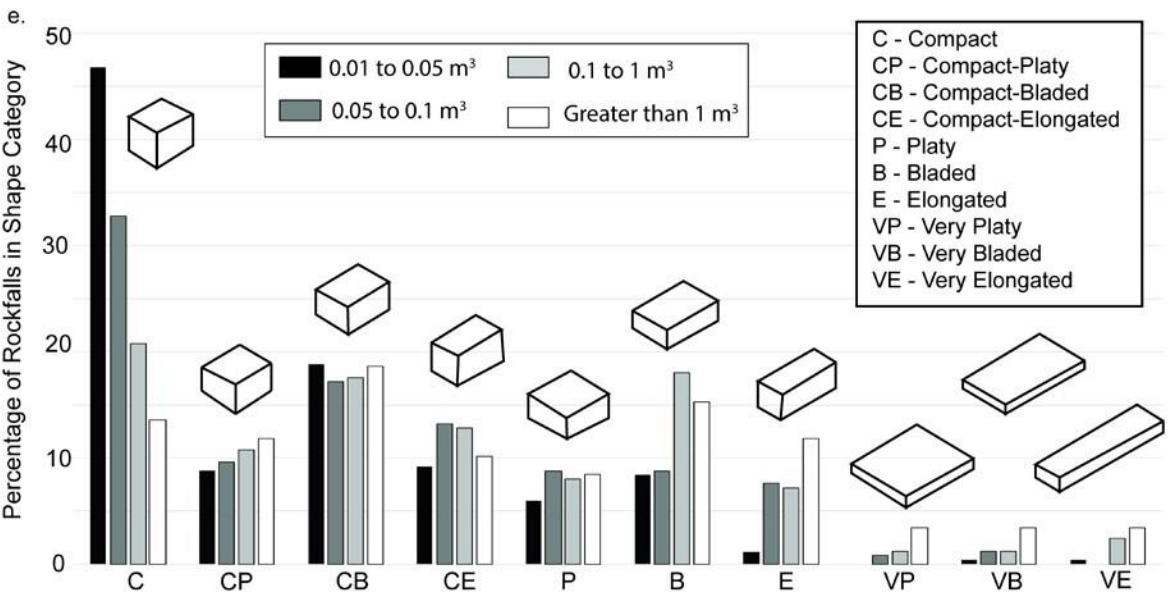
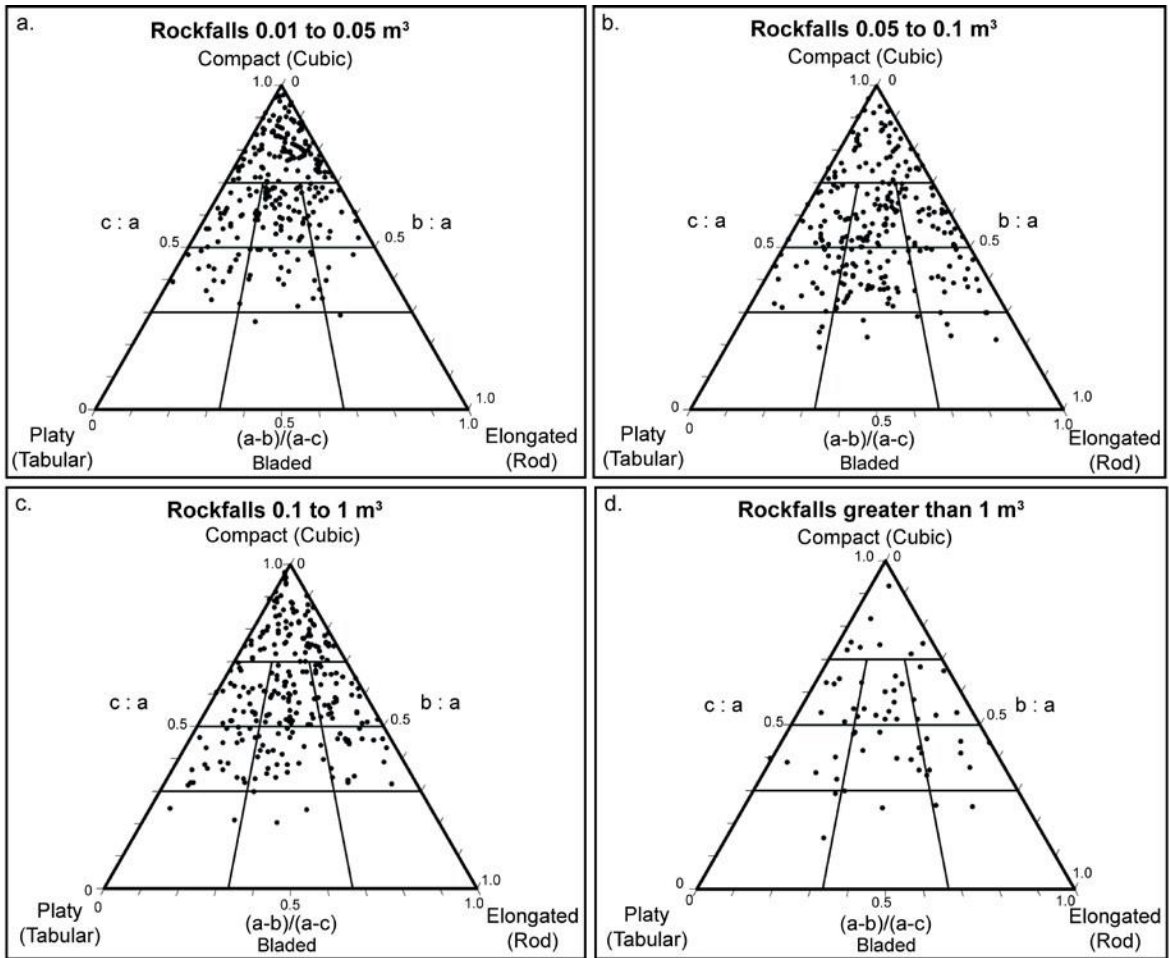
11

12

13

24

Fig. 13



1  
3  
4

Fig. 14

